

## Accepted Manuscript

Fluorescent rhodanine-3-acetic acids visualize neurofibrillary tangles in Alzheimer's disease brains

Upendra Rao Anumala, Jiamin Gu, Fabio Lo Monte, Thomas Kramer, Roland Heyny-von Haußen, Jana Hölzer, Valerie Goetschy-Meyer, Christian Schön, Gerhard Mall, Ingrid Hilger, Christian Czech, Jochen Herms, Boris Schmidt

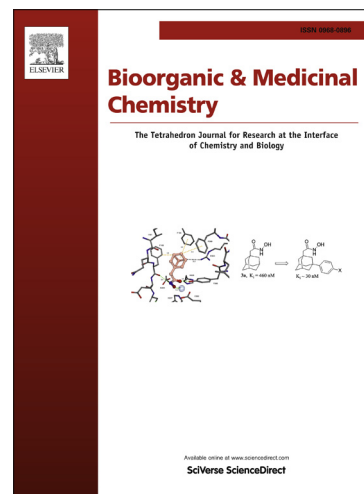
PII: S0968-0896(13)00570-1  
DOI: <http://dx.doi.org/10.1016/j.bmc.2013.06.039>  
Reference: BMC 10932

To appear in: *Bioorganic & Medicinal Chemistry*

Received Date: 26 April 2013  
Revised Date: 11 June 2013  
Accepted Date: 16 June 2013

Please cite this article as: Anumala, U.R., Gu, J., Monte, F.L., Kramer, T., Haußen, R.H-v., Hölzer, J., Goetschy-Meyer, V., Schön, C., Mall, G., Hilger, I., Czech, C., Herms, J., Schmidt, B., Fluorescent rhodanine-3-acetic acids visualize neurofibrillary tangles in Alzheimer's disease brains, *Bioorganic & Medicinal Chemistry* (2013), doi: <http://dx.doi.org/10.1016/j.bmc.2013.06.039>

This is a PDF file of an unedited manuscript that has been accepted for publication. As a service to our customers we are providing this early version of the manuscript. The manuscript will undergo copyediting, typesetting, and review of the resulting proof before it is published in its final form. Please note that during the production process errors may be discovered which could affect the content, and all legal disclaimers that apply to the journal pertain.





## Fluorescent rhodanine-3-acetic acids visualize neurofibrillary tangles in Alzheimer's disease brains

Upendra Rao Anumala<sup>a</sup>, Jiamin Gu<sup>a,†</sup>, Fabio Lo Monte<sup>a,‡</sup>, Thomas Kramer<sup>a</sup>, Roland Heyny-von Haußen<sup>b</sup>, Jana Hölzer<sup>c</sup>, Valerie Goetschy-Meyer<sup>d</sup>, Christian Schön<sup>e</sup>, Gerhard Mall<sup>b</sup>, Ingrid Hilger<sup>c</sup>, Christian Czech<sup>d</sup>, Jochen Herms<sup>e</sup>, Boris Schmidt<sup>a,\*</sup>

<sup>a</sup>Clemens Schöpf-Institute of Chemistry and Biochemistry, Technische Universität Darmstadt, Petersenstrasse 22, 64287, Darmstadt, Germany

<sup>b</sup>Institute of Pathology, Klinikum Darmstadt, Grafenstrasse 9, Darmstadt 64283, Germany

<sup>c</sup>Institute of Diagnostic and Interventional Radiology I, Jena University Hospital – Friedrich Schiller University Jena, Erlanger Allee 101, 07747 Jena, Germany

<sup>d</sup>F. Hoffmann-La Roche AG, Grenzachstrasse 124, Gebäude 93/3.44, Basel 4070, Switzerland

<sup>e</sup>Department of Translational Brain Research, DZNE, German Center for Neurodegenerative Diseases, Munich, Germany

\*Corresponding author. Tel.: +49 6151 164531; fax: +49 6151 163278.

E-mail address: schmidt\_boris@t-online.de (B. Schmidt).

<sup>†</sup>Present address: Alberta Glycomics Centre, Department of Chemistry, University of Calgary, 2500 University Drive NW, Calgary Alberta T2N 1N4, Canada

<sup>‡</sup>Present address: Institute of Organic Chemistry, University of Zurich, Winterthurerstrasse 190, CH-8057, Zurich, Switzerland

### ARTICLE INFO

#### Article history:

Received

Received in revised form

Accepted

Available online

#### Keywords:

Alzheimer's disease

Neurofibrillary tangles

Zebrafish

Cytotoxicity

Fluorescence imaging

### ABSTRACT

There is a high demand for the development of an imaging agent for neurofibrillary tangles (NFTs) detection in Alzheimer's diagnosis. In the present study, a series of rhodanine-3-acetic acids was synthesized and evaluated for fluorescence imaging of NFTs in brain tissues of AD patients. Five out of seven probes have shown excellent binding affinity to NFTs over amyloid plaques in the *Thiazine red R* displacement assay. However, the selectivity in this *in vitro* assay is not confirmed by the histopathological evaluation, which indicates significant differences in the binding sites in the assays. Probe 6 showed binding affinity ( $IC_{50} = 19$  nM) to tau aggregates which is the highest among this series. Probes 2, 3, 4 and 5 display  $IC_{50}$  values of lower than 100 nM to tau aggregates to displace *Thiazine red R*. Evaluation of the cytotoxicity of these five probes with human liver carcinoma cells revealed that these compounds exert negligible cytotoxicity. The *in vivo* studies with zebrafish embryos confirmed negligible cytotoxicity at 24 and 72 hours post fertilization.

2009 Elsevier Ltd. All rights reserved.

### 1. Introduction

Alzheimer's disease (AD) is one of the most common forms of dementia. This disease is a progressive neurodegenerative disorder associated with cognitive decline, disorientation and language impairment. Incidence of new AD cases worldwide is growing with the age of the baby boomer generation.<sup>1, 2</sup> The major cause is still unknown for the disease but it is usually accepted that the formation of two abnormal proteins; extra cellular senile plaques (SPs) and neurofibrillary tangles (NFTs) are the two key pathological findings in postmortem histology. They are observed in hippocampus and cerebral cortex but also in other areas of the brain. SPs are composed of aggregated  $\beta$ -amyloid ( $A\beta$ ) peptides and NFTs are formed by the aggregated microtubule associated tau protein.<sup>3</sup>

Non-invasive imaging is vital for early diagnosis of AD. Currently there are few positron emission tomography (PET) imaging agents available for the early diagnosis. PET imaging is a very well-known technique which provides good sensitivity

deep in tissue.<sup>4</sup> Nevertheless it is limited by a time-consuming

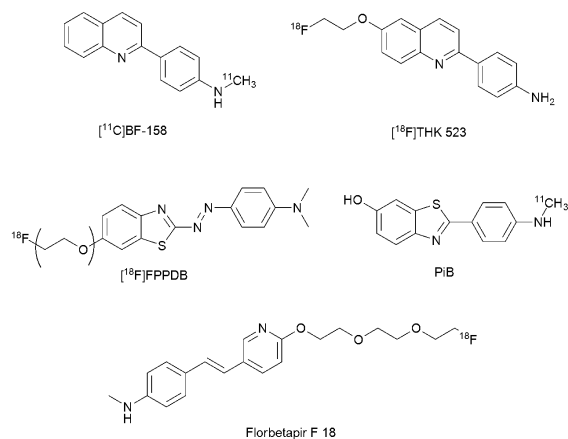


**Figure 1.** Structure of PET imaging probes for the detection of NFTs and  $A\beta$  plaques in AD brain tissues

**Table 1**

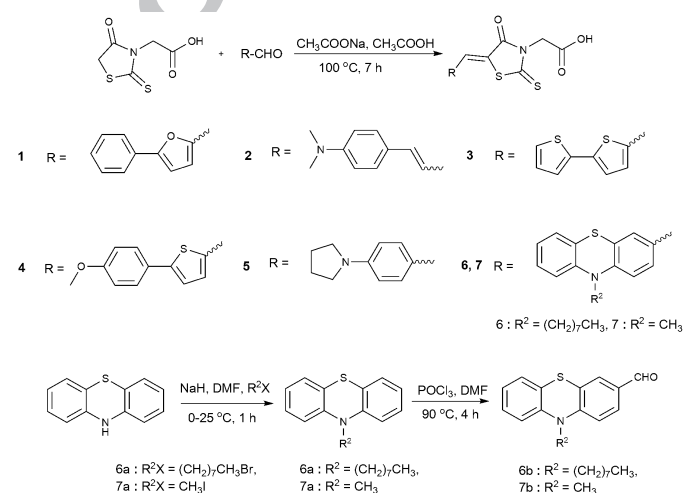
General properties, optical properties, competitive *Thiazine Red R* displacement from tau-/A $\beta$ <sub>40</sub>-aggregates for probes **1-7** and cytotoxicity.

Compound	Yield <sup>a</sup>	M.Wt <sup>b</sup>	cLogP <sup>c</sup>	$\lambda_{\max}^{\text{abs}}$ (nm) <sup>d</sup>	$\lambda_{\max}^{\text{em}}$ (nm) <sup>d</sup>	Aggr. Tau- IC <sub>50</sub> /nM	Aggr. A $\beta$ <sub>40</sub> - IC <sub>50</sub> /nM	Cytotox. EC <sub>50</sub> ( $\mu$ M) <sup>e</sup>
<b>1</b>	79	345.39	2.70	445	511	662	5002	>100*
<b>2</b>	61	348.44	2.19	497	645	32	55	>100*
<b>3</b>	53	367.49	3.03	444	525	43	292	>100*
<b>4</b>	83	391.48	3.11	391	533	28	91	>100*
<b>5</b>	85	348.44	1.70	468	555	63	218	>100*
<b>6</b>	71	512.71	7.12	466	651	19	91	18
<b>7</b>	69	414.52	3.41	455	645	238	1156	>100*

<sup>a</sup> Isolated yields <sup>b,c</sup> Determined by CS Chemoffice 10.0. <sup>d</sup> Measured in ethanol. <sup>e</sup> EC<sub>50</sub> declares the dye concentration in which 50% of the cells died after incubation with the probe after 24 h of exposure. \* a decrease of cell viability  $\geq$  50% was not observed at the tested concentrations. The IC<sub>50</sub> data were obtained from the average of technical replicates and are thus presented without standard deviation

data acquisition process and exposure to radioactivity, insufficient spatial resolution along with expensive equipment and need of highly skilled personnel. Pittsburgh compound B (PiB) and Flortetapir F18 are well studied PET ligands targeting SPs.<sup>5,6</sup> Flortetapir F18 is a PET probe for the imaging of A $\beta$  plaque density in AD patients and other causes of cognitive decline.<sup>7</sup> Flortetapir is the most widely used amyloid marker for A $\beta$  PET-imaging. PET ligands for imaging of NFTs were also reported. These include [<sup>11</sup>C]-BF-158, [<sup>18</sup>F]-THK 523 and [<sup>18</sup>F]-FPPDB (Figure 1).<sup>8-10</sup> Moreover, A $\beta$  imaging cannot differentiate between different forms of frontotemporal lobe degeneration and A $\beta$  plaque load plateaus as disease progresses. Additionally, PIB imaging is negative in up to 25% of the patients diagnosed with AD.<sup>11</sup> Furthermore, the formation of neurofibrillary tangles brain correlates better with disease progression in AD.<sup>12</sup> Fluorescence imaging is a relatively new modality that offers real time, non-radioactive, inexpensive *in vivo* imaging.<sup>13</sup> It is frequently rejected to be a non-viable modality in humans, however the recent reports on pathological changes in the retina and the human olfactory system suggest to investigate a non-invasive access to amyloid and tau deposits by either scanning of the retina or endoscopic nasal examination.<sup>14,15</sup>

Fluorescence imaging of a boron dipyrromethane derivative (BAP-1) and curcumin has been reported for A $\beta$  deposits.<sup>16</sup> The



**Scheme 1.** Synthesis of rhodanine-3-acetic acids and 10-alkyl-10H-phenothiazine-3-carbaldehyde.

presence of hyperphosphorylated non-fibrillar tau was reported for both the retina of P301S transgenic mice and the human retina.<sup>17</sup> Thus, there is an immediate need for fluorescent NFT-imaging agents, which may complement the established amyloid PET imaging tools.

Rhodanine based compounds are known for their ability to inhibit tau aggregation *in vitro* and *in vivo*.<sup>18-20</sup> Rhodanine and thiohydantoin derivatives were reported as single photon emission computed tomography (SPECT) imaging agents for NFTs.<sup>21</sup> Rhodanine-3-acetic acids are known as amyloid imaging agents, dye sensitized solar cells and anthrax lethal factor protease inhibitors.<sup>22-25</sup> In the present study we synthesized and studied the fluorescence imaging properties of rhodanine-3-acetic acid (RA) derivatives as fluorescent probes for NFTs and evaluated their affinities in the *Thiazine red R* assay. We evaluated the effects of these probes on cell metabolism on human hepato-cellular carcinoma cells (HepG2) and zebrafish embryo development. These compounds were evaluated in human and transgenic P301 mice retinae for their ability as imaging agents. However, the absence of fibrillar tau deposits in the retina of both species excluded a proof of concept.<sup>17</sup>

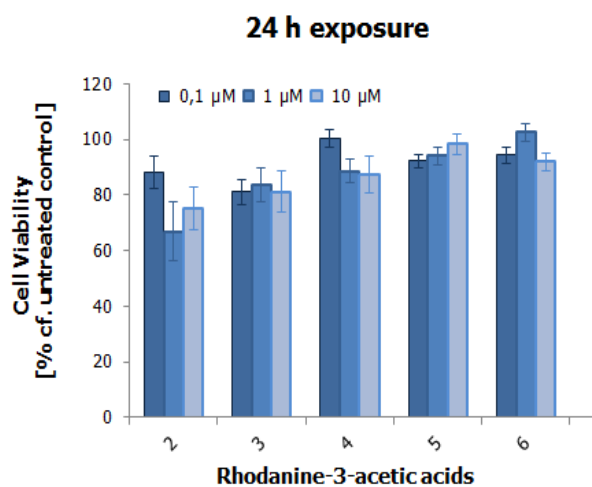


**Figure 2.** Cell viabilities of HepG2 cells after 24 hours of exposure with the probes **2** to **6** at 0.1, 1 and 10  $\mu$ M concentrations after 24 hours of exposure. +/- SD

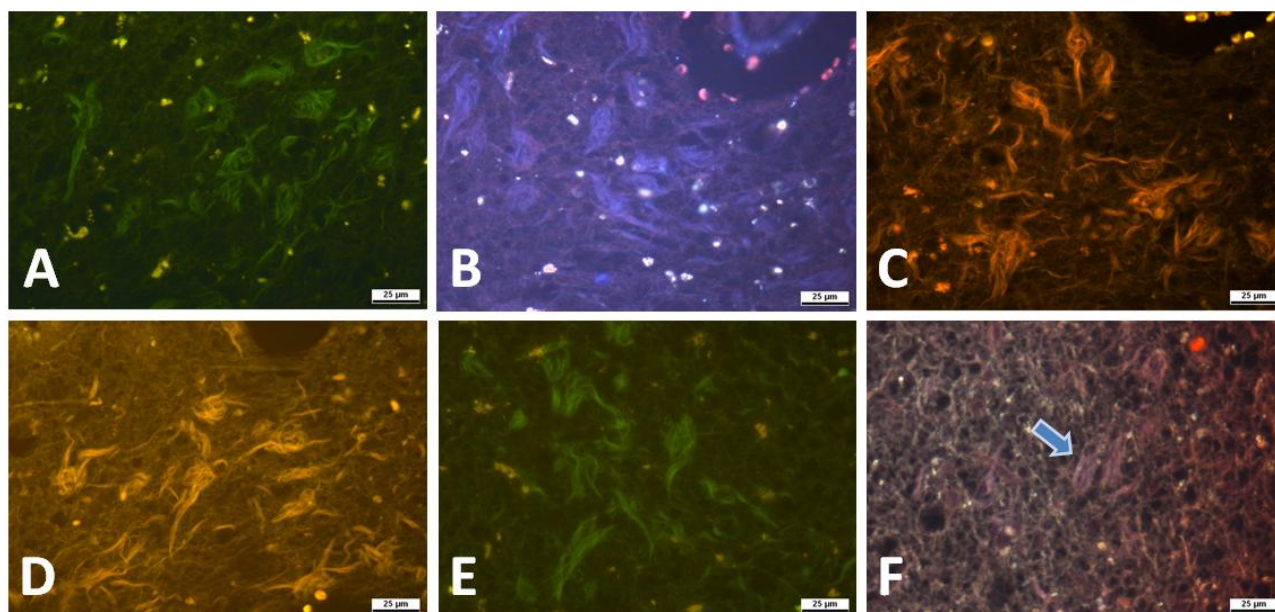


**Figure 3.** Neuropathological staining of brain sections from the hippocampus of an AD patient (A-F). Probe **1** (A), **2** (B), **3** (C), **4** (D), **5** (E) clearly stained flame shaped neurofibrillary tangles and Probe **6** (F) showed photo bleaching and high background tissue staining to NFTs. (NFTs are shown with arrow). Tissues: hippocampus; patient: female, 80 years old, CERAD Score: 3; NFTs-level: V.

## 2. Results and discussion

RA derivatives were synthesized by known methods using a Knoevenagel condensation between RA and corresponding aldehydes using sodium acetate in acetic acid.<sup>26</sup> Most of the aldehydes used in the present study were commercial but a few aldehydes had to be synthesized by known methods. Probes **6** and **7** were synthesized in a three step procedure. In the first step, alkylation of phenathiazine in the presence of sodium hydride and dimethyl formamide was performed. The *N*-alkyl phenathiazine was formylated in the second step employing the Vilsmeier-Haack reaction of phosphorous oxychloride and dimethylformamide. In the final step a Knoevenagel condensation was carried out between the RA derivatives and *N*-alkyl phenathiazine aldehyde to obtain the probes **6** and **7**. The yields of the Knoevenagel condensation for probes **1-7** varied from 61-85% depending on the aldehydes. The presence of electron donating groups increased the reactivity whereas electron withdrawing groups decreased the reactivity and yield of derivative formation.

All of these compounds were further evaluated for their ability to visualize NFTs in *post mortem* human AD brain sections.

Initial immune histochemical staining confirmed that these tissues contain both NFTs and SPs (supporting info). The RA derivatives were used to stain these protein aggregates on brain sections of the same patient. All of these compounds showed selective binding to NFTs of *post mortem* AD brain tissues. Our observations with RA derivatives showed selective staining to NFTs rather than that of A $\beta$  plaques, which stands in contrast with the selectivity observed in the *Thiazine red R* displacement assay. This striking difference indicates a significant difference between the binding sites in the protein aggregation assay and the human brain. A related discrepancy was reported for amyloid binding agents in filtration assays and upon binding to human tissue.<sup>27</sup> Thus the affinity data obtained from the displacement assays must be analyzed with care. The introduction of a bis-thiophene moiety on RA leads to probe **3**, which displayed good fluorescence. Under the fluorescence microscope, this compound displayed excellent staining of NFTs in brain tissues. Most of these compounds showed reduced background staining in comparison to the staining of NFTs. Probe **1** stained NFTs in good contrast to the background, whereas photo bleaching was observed with probe **6**. (Figure 3).

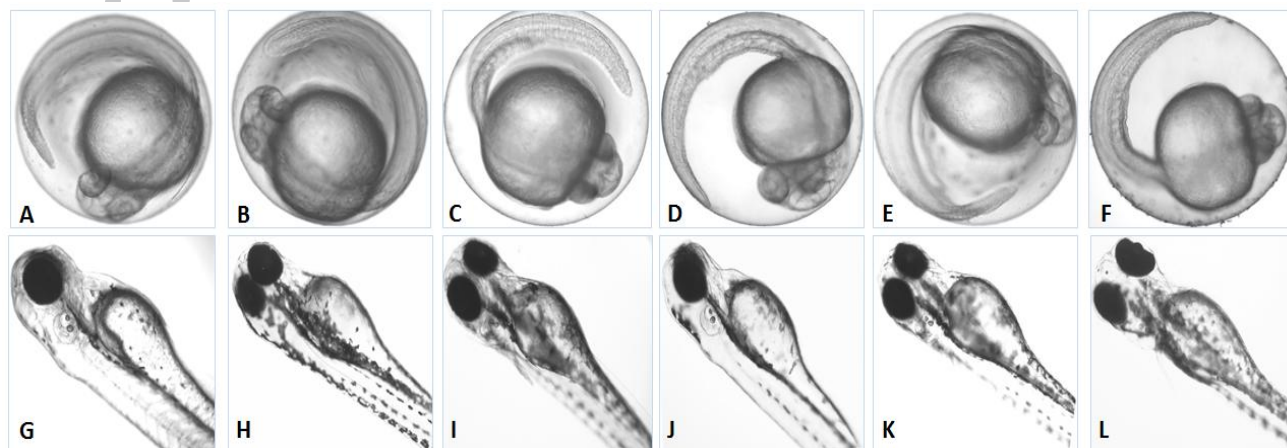


**Figure 4.** *In vivo* cytotoxicity studies with embryos of zebrafish after 24 (A-F) and 72 (G-L) hpf. Controls (A and G), Probe **2** (B and H), **3** (C and I), **4** (D and J), **5** (E and K) at 10  $\mu$ M concentration and Probe **6** (F and L) at 5  $\mu$ M concentration.

The *in vitro* affinity studies of these compounds were performed by the *Thiazine red R* displacement assay.<sup>15, 28, 29</sup> *Thiazine red R* is known for its binding to tau aggregates *in vitro* and for its superiority over *Thioflavin T*.<sup>30</sup> Aggregates of recombinant human-microtubule associated tau protein, which was purified from *Escherichia coli*, and synthetic A $\beta$  peptides were used in this study. The *in vitro* aggregates of A $\beta$ <sub>40</sub> and A $\beta$ <sub>42</sub> display differences in the binding sites for amyloid ligands, which depend on the aggregation conditions and differ from the binding situation observed in human tissue. Thus we selected A $\beta$ <sub>40</sub> for the aggregation assay as it is the predominant component in amyloid plaques and thus likely to be engaged in binding of the probes.

IC<sub>50</sub> values of *Thiazine red R* are depicted in Table 1. All of these probes have higher affinity to aggregated tau than aggregated A $\beta$ <sub>40</sub> in the *Thiazine red R* assay. However, the apparent selectivity in the histology was even higher than indicated by the affinity assays. This suggests fundamental differences between the protein aggregates. Caveat: chemically induced synthetic tau fibrils are not a reliable surrogate for native NFTs, they differ in size, morphology and binding properties.<sup>31</sup> Five compounds out of seven showed IC<sub>50</sub> values of less than 100 nM. Probe **6** showed almost five fold higher affinity to tau aggregates (19 nM) than to amyloid- $\beta$  aggregates (91 nM), the highest selectivity to tau aggregates in this series. Probe **3** showed around 7-fold higher affinity to aggregated tau but weaker binding in comparison to probe **6**.

Probes **2**, **3**, **4** and **5** displayed IC<sub>50</sub> values of 32 nM, 43 nM, 28 nM and 63 nM, respectively. Probes **1** and **7** display poor affinity compared to the other probes in this series. Apparently, the binding affinities of RA derivatives are higher to tau aggregates than to A $\beta$ <sub>40</sub> aggregates. It is generally known that compounds with a *cLogP* lesser than 3 and a molecular weight less than 500 Daltons are most favourable for blood brain barrier (BBB) penetration.<sup>32</sup> RA derivatives were designed according to these *cLogP* values. According to the *cLogP* value, Probe **5** (*cLogP* value of 1.7) has the lowest *cLogP* value in this series and other probes except probe **6** are in the range of 2.0 to 3.5. Probe **6** is characterized by a *cLogP* of 7.12. Despite the high affinity of probe **6** to tau aggregates the lipophilicity, poor solubility and photo bleaching make it unsuitable for *in vivo* studies.

As safety is one of the most important factors during the development of an imaging agent, the effects of these compounds on HepG2 cell proliferation and zebrafish embryo development were evaluated. Except for probes **1** and **7**, all other probes were tested for their cytotoxicity in zebrafish embryos. The cytotoxicity evaluation of probes **2-5** clearly showed that most of these probes have no or negligible cytotoxicity at concentrations up to 10  $\mu$ M. Probe **6** showed cytotoxicity at 10  $\mu$ M concentration. Yet, no lesions in embryos of zebrafish were observed at 5  $\mu$ M concentration at 24 and 72 hours post fertilization (hpf), which indicates that all of these compounds display negligible cytotoxicity up to a concentration of 5  $\mu$ M. It was observed that zebrafish embryos developed normally in comparison with control for all RA derivatives at 5  $\mu$ M. Further experiments with liver HepG2 cells were performed and the effective doses (EC<sub>50</sub>) were calculated via the best-fitted trend line of cell viability as a function of dye concentration. Probes within the range of 1-100 nM affinity to tau aggregates were considered for the cytotoxicity studies. Probes **2**, **3**, **4**, **5** and **6** were studied *in vitro* for their cytotoxicity in HepG2 cells. Apart from compound **6**, the EC<sub>50</sub> values of all compounds are > 100  $\mu$ M and loss of cell viability  $\geq$  50 % was not observed at the

tested concentrations (100  $\mu$ M was the highest concentration tested). The EC<sub>50</sub> of probe **6** after 24 h of incubation is about 18  $\mu$ M. Figure 2 shows the cell viability of these compounds in HepG2 cells at 24 h after incubation.

It was recently reported that fibrillar tau inclusions can be observed in retinal ganglion cells of P301S mice *in* and *ex vivo*.<sup>17, 33</sup> However, we could not visualize fibrillar tau aggregates with these compounds (Probe **1**, **2**, **3** and **4**) in the retina of P301S mice. These results suggest that the tau aggregates in the retina of P301S mice may be distinctly different from human tau aggregates that can be stained with compounds **1-4**. This may be due to the fact that the human brain produces a mixture of 3R and 4R isoforms of tau, whereas the P301S mice do produce one isoform only.

### 3. Conclusion

In summary, RA derivatives provide selective visualization of NFTs over A $\beta$  plaques in brain sections of *post mortem* AD patient. Excellent affinity to fibrillar tau aggregates was observed in the *Thiazine red R* displacement assay and no or negligible cytotoxicity of these compounds in HepG2 cells or in zebrafish embryo development. Hyperphosphorylated, non-fibrillar Tau aggregates as present in aggresomes or mouse retina are not stained by these dyes, this observation indicates selective binding to fibrillar tau. Further evaluation of these compounds is needed in mammals that produce a similar isoform mixture of tau aggregates as humans.

## 4. Experimental

### 4.1. General

All commercial chemicals, reagents, solvents were purchased from Sigma-Aldrich. All reactions were performed under argon atmosphere using dry solvents unless otherwise specified. <sup>1</sup>H-NMR spectra were recorded on a Bruker AC300, ARX300 and DRX 500 spectrometer at 300 MHz and 500 MHz respectively. The <sup>13</sup>C-NMR spectra were recorded on a Bruker AC300, ARX300 and DRX 500 spectrometer at 75 MHz and 125 MHz respectively. Chemical shifts values were reported as  $\delta$  values (ppm) downfield from Me<sub>4</sub>Si. UV-Vis spectra were carried out by Shimadzu UV-2401PC. Fluorescence emission experiments were carried out by TECAN Infinite® M1000 PRO. Mass spectrometry was performed on a MAT 95 double focusing sector field MS. Flash column chromatography was carried out with Merck silica gel 60 (15-40 mm). Acid protons are not visible in <sup>1</sup>H-NMR for some compounds measured in DMSO-d<sub>6</sub>.

### 4.2. General procedure for the synthesis of RA derivatives

#### 4.2.1. (Z)-2-(4-Oxo-5-((5-phenylfuran-2-yl)methylene)-2-thioxothiazolidin-3-yl)acetic acid (**1**)

To a solution of 5-phenylfuran-2-carbaldehyde (1.0 mmol, 1 equiv.) and rhodanine-3-acetic acid (1.0 mmol, 1 equiv) in glacial acetic acid (5 ml) was added of sodium acetate (3.0 mmol, 3 equiv) and the reaction mixture was stirred for 7 hours at 100°C, forming a precipitate after cooled to room temperature. The resulted crude product was recovered by filtration and recrystallized from acetone/water mixture to give 272 mg of the titled compound as an orange solid; <sup>1</sup>H-NMR (500 MHz, DMSO-d<sub>6</sub>)  $\delta$  = 13.42 (s, 1H), 7.91 – 7.85 (m, 2H), 7.77 (s, 1H), 7.61 – 7.55 (m, 2H), 7.49 – 7.44 (m, 1H), 7.42 (d, *J* = 3.8 Hz, 1H), 7.36 (d, *J* = 3.8 Hz, 1H), 4.75 (s, 2H); <sup>13</sup>C-NMR (125 MHz, DMSO-d<sub>6</sub>)  $\delta$  = 194.24, 167.78, 166.48, 158.78, 149.61, 129.91, 129.85, 128.97, 124.96, 124.18, 119.62, 118.28, 110.84, 45.46;

MS (EI, 70 eV)  $m/z = 345 [M^+]$ ; UV/Vis (Ethanol)  $\lambda_{\max} = 445$  nm.

#### 4.2.2. 2-((Z)-5-((E)-3-(4-(dimethylamino)phenyl)allylidene)-4-oxo-2-thioxothiazolidin-3-yl)acetic acid (2)

Further purification of this compound was carried out using column chromatography. A red solid;  $^1\text{H-NMR}$  (500 MHz, DMSO- $d_6$ ):  $\delta = 7.58$  (dd,  $J = 7.2, 4.8$  Hz, 3H), 7.35 (d,  $J = 14.8$  Hz, 1H), 6.87 – 6.78 (m, 1H), 6.74 (d,  $J = 9.0$  Hz, 2H), 4.69 (s, 2H), 3.02 (s, 6H);  $^{13}\text{C-NMR}$  (125 MHz, DMSO- $d_6$ ):  $\delta = 192.84, 167.89, 166.03, 152.34, 148.57, 136.69, 130.91, 123.49, 118.62, 118.53, 112.35, 45.37, 39.65$  (NMe<sub>2</sub> peak un resolved from DMSO); HRMS  $m/z [M^+]$  calcd for C<sub>16</sub>H<sub>16</sub>N<sub>2</sub>O<sub>3</sub>S<sub>2</sub><sup>+</sup>: 348.0602, found 348.0603; UV/Vis (Ethanol)  $\lambda_{\max} = 497$  nm.

#### 4.2.3. (Z)-2-(5-(2,2'-Bithiophen-5-ylmethylene)-4-oxo-2-thioxothiazolidin-3-yl)acetic acid (3)

A brick red solid;  $^1\text{H-NMR}$  (500 MHz, DMSO- $d_6$ )  $\delta = 8.14$  (s, 1H), 7.78 (dd,  $J = 4.0, 0.5$  Hz, 1H), 7.70 (dd,  $J = 5.0, 1.0$  Hz, 1H), 7.59 (dd,  $J = 3.7, 1.0$  Hz, 1H), 7.54 (d,  $J = 4.0$  Hz, 1H), 7.18 (dd,  $J = 3.6, 1.4$  Hz, 1H), 4.73 (s, 2H);  $^{13}\text{C-NMR}$  (125 MHz, DMSO- $d_6$ )  $\delta = 192.18, 167.72, 166.41, 145.64, 138.39, 136.11, 135.66, 129.40, 128.52, 127.12, 126.91, 126.32, 118.98, 45.63$ ; MS (EI, 70 eV)  $m/z = 367 [M^+]$ ; UV/Vis (Ethanol)  $\lambda_{\max} = 444$  nm.

#### 4.2.4. (Z)-2-(5-((5-(4-Methoxyphenyl)thiophen-2-yl)methylene)-4-oxo-2-thioxothiazolidin-3-yl)acetic acid (4)

A maroon solid;  $^1\text{H-NMR}$  (500 MHz, DMSO- $d_6$ )  $\delta = 8.08$  (s, 1H), 7.77 (d,  $J = 4.5$  Hz, 1H), 7.75 (d,  $J = 8.7$  Hz, 2H), 7.64 (d,  $J = 4.0$  Hz, 1H), 7.03 (d,  $J = 8.7$  Hz, 2H), 4.56 (s, 2H), 3.82 (s, 3H);  $^{13}\text{C-NMR}$  (125 MHz, DMSO- $d_6$ )  $\delta = 192.33, 167.35, 166.70, 160.67, 152.66, 138.38, 135.88, 127.88, 126.74, 125.62, 125.11, 118.96, 115.26, 55.86, 46.98$ ; MS (EI, 70 eV):  $m/z = 391 [M^+]$ ; UV/Vis (Ethanol):  $\lambda_{\max} = 451$  nm.

#### 4.2.5. (Z)-2-(4-Oxo-5-(4-(pyrrolidin-1-yl)benzylidene)-2-thioxothiazolidin-3-yl)acetic acid (5)

A maroon solid;  $^1\text{H-NMR}$  (500 MHz, DMSO- $d_6$ ):  $\delta = 7.69$  (s, 1H), 7.49 (t,  $J = 5.8$  Hz, 2H), 6.71 (t,  $J = 5.9$  Hz, 2H), 4.54 (s, 2H), 3.36 (t,  $J = 6.6$  Hz, 4H), 1.99 (t, 4H);  $^{13}\text{C-NMR}$  (125 MHz, DMSO- $d_6$ ):  $\delta = 192.94, 167.39, 167.13, 149.93, 135.24, 133.84, 120.04, 113.81, 112.97, 47.86, 46.82, 25.37$ ; MS (EI, 70 eV):  $m/z = 348 [M^+]$ ; UV/Vis (Ethanol):  $\lambda_{\max} = 468$  nm.

#### 4.2.6. (Z)-2-(5-((10-Octyl-10H-phenothiazin-3-yl)methylene)-4-oxo-2-thioxothiazolidin-3-yl)acetic acid (6)

A maroon solid;  $^1\text{H-NMR}$  (500 MHz, DMSO- $d_6$ )  $\delta = 7.77$  (s, 1H), 7.48 (dd,  $J = 8.8, 2.2$  Hz, 1H), 7.40 (d,  $J = 2.1$  Hz, 1H), 7.25 – 7.20 (m, 1H), 7.18 – 7.14 (m, 2H), 7.09 – 7.05 (m, 1H), 7.00 (td,  $J = 7.5, 1.0$  Hz, 1H), 4.73 (s, 2H), 3.93 (t,  $J = 7.0$  Hz, 2H), 1.73 – 1.64 (m, 2H), 1.43 – 1.34 (m, 2H), 1.30 – 1.17 (m, 8H), 0.82 (t,  $J = 6.9$  Hz, 3H);  $^{13}\text{C-NMR}$  (125 MHz, DMSO- $d_6$ )  $\delta = 193.17, 167.75, 166.78, 147.71, 143.43, 133.58, 131.30, 129.95, 128.42, 127.71, 127.37, 124.38, 123.94, 122.68, 119.04, 116.86, 116.62, 47.30, 45.49, 31.53, 29.03, 28.89, 26.51, 26.39, 22.47, 14.39$ ; MS (EI, 70 eV):  $m/z = 512.0 [M^+]$ ; UV/Vis (Ethanol)  $\lambda_{\max} = 466$  nm.

#### 4.2.7. (Z)-2-(5-((10-Methyl-10H-phenothiazin-3-yl)methylene)-4-oxo-2-thioxothiazolidin-3-yl)acetic acid (7)

A dark red solid;  $^1\text{H-NMR}$  (500 MHz, DMSO- $d_6$ )  $\delta = 7.79$  (s, 1H), 7.51 (dd,  $J = 2.20, 8.59$  Hz, 1H), 7.43 (d,  $J = 2.17$  Hz, 1H), 7.26 (td,  $J = 1.60, 7.70$  Hz, 1H), 7.19 (dd,  $J = 1.56, 7.82$  Hz, 1H), 7.11 (d,  $J = 8.62$  Hz, 1H), 7.03 (dd,  $J = 5.68, 8.03$  Hz, 2H), 4.73 (s, 2H), 3.39 (s, 3H);  $^{13}\text{C-NMR}$  (125 MHz, DMSO- $d_6$ ):

$\delta = 192.70, 167.25, 166.28, 147.68, 143.72, 133.13, 130.98, 129.11, 128.08, 126.99, 126.92, 123.45, 122.86, 120.99, 118.69, 115.32, 115.20, 45.02, 35.50$ ; MS (EI, 70 eV)  $m/z = 414 [M^+]$ ; UV/Vis (Ethanol)  $\lambda_{\max} = 455$  nm.

### 4.3. Methods

#### 4.3.1. Immunohistochemical staining

Immunohistochemical staining was carried out on four micrometers thick sections of the AD patient tissues by a Ventana Benchmark automated stainer (Ventana, Tuscon, AZ). The antibodies are anti-PHF-Tau 75 clone AT8 mAb (Thermo Scientific Pierce Protein Research Products, Rockford, IL), TAU Ab-3 (Neomarkers, Fremont, CA), and amyloid A4 (BAM10, Sigma, St. Louis, MO) and the Ultraview Universal DAB Detection Kit (Ventana, Tuscon, AZ) were used in staining experiments.

#### 4.3.2. Neuropathological staining of AD brain sections

*Post mortem* brain tissues from an AD patient (80-year old female) were obtained at autopsy. Four micrometer thick paraffin embedded serial sections of the hippocampus area were deparaffinized with xylene and ethanol. These sections were then hydrated in distilled water. Ethanol solution (500  $\mu\text{L}$ ) of probes **1** to **7** with concentration of 1 mM was poured on tissue slide and waited for 10 min. These sections were washed with methanol and differentiated in 1% acetic acid solution for 20 min and washed with water. These tissue sections were finally treated with Roti – Mount Fluor Care (from Sigma-Aldrich) and covered with coverslip. Fluorescence microscopic examination was performed using a Axioskop microscope with a HBO100 fluorescence illuminator (Carl Zeiss, Oberkochen, Germany) with band pass filter set 09 BP450-490, FT510, LP515, the filter set 02 G365, FT395, LP420 and the filter set 15 BP546, FT580, LP590.

#### 4.3.3. In vitro cell proliferation assay

The cytotoxicity data were determined via CellTiter 96<sup>®</sup>AQueous non-radioactive cell proliferation assay (Promega, Madison, USA), which is based on the reduction of a tetrazolium salt [3-(4,5-dimethylthiazol-2-yl)-5-(3-carboxymethoxy phenyl)-2-(4-sulfophenyl)-2H-tetrazolium, inner salt; MTS] into a formazan product by intrinsic dehydrogenases of living cells.

In short, human liver hepatocellular carcinoma cells HepG2, maintained in DMEM/F12 1+1 and supplemented with 10 % fetal bovine serum, were seeded in 96-well plates and incubated with 0.1  $\mu\text{M}$ , 1  $\mu\text{M}$ , 10  $\mu\text{M}$  and 100  $\mu\text{M}$  of probe **2**, **3**, **4**, **5** and **6** for 24 hours. After washing, CellTiter 96<sup>®</sup>AQueous non-radioactive cell proliferation assay reagent was added to the cells and the number of metabolically active cells was calculated by measuring the amount of formazan product via photometric analysis at  $\lambda = 492$  nm. The absorbance of treated samples was normalized to untreated controls (percent of non-treated controls), which resulted in cell viability. Finally effective doses (EC<sub>50</sub>) that induced a loss in cell viability of 50 % were calculated via the best-fitted trend line of cell viability as a function of dye concentration.

#### 4.3.4. Thiazine Red R displacement assay

Recombinant human-microtubule associated 4R tau protein purified from Escherichia coli and Synthetic A $\beta$ <sub>40</sub> was used in this assay. Tau protein was aggregated at 5  $\mu\text{M}$  concentration with arachidonic acid (100  $\mu\text{M}$ ) in Tris 10 mM pH = 8, 24h at 37°C, whereas A $\beta$ <sub>40</sub> was aggregated at a concentration of 50  $\mu\text{M}$  with arachidonic acid (100  $\mu\text{M}$ ) in Tris 10 mM pH = 8, for three

days at 37°C. For the displacement assay, *Thiazine red R* was added at same concentration of the *Kd* to the respective aggregated binding sites ( $K_d$  for aggregated Tau = 18 nM,  $K_d$  for aggregated A $\beta$  = 49 nM). To determine the affinity of the required probe, the probe was added at different concentrations in the assay ranging from 0.1 nM to 10000 nM. Auto fluorescence of the probe was measured together with aggregated proteins. Negative controls were obtained from *Thiazine red R* and aggregated proteins. Assay was performed in Perkin Elmer OptiPlate 384, black, 45  $\mu$ l assay volume, assay buffer was DPBS no CaCl<sub>2</sub> no MgCl<sub>2</sub> (GIBCO N. 14020). Tested compounds were diluted in DMSO and 2.25  $\mu$ l was added to the assay (5% DMSO final). Assay experiment was initiated by the addition of the aggregated protein (competitive condition). Plates were shortly shacked (1 min with Sterico variomag teleshake) and incubated for 30 min at room temperature. Measurements were performed with En:Vision (Perkin Elmer), at excitation 531 nm/emission 595 nm. Corresponding IC<sub>50</sub> were calculated by excel fit.

#### 4.3.5. *In vivo* zebrafish embryo development assay

Zebra fish were bred in 2L spawning tank and maintained according to the methods described by Christiane Nuesslein-Volhard and Ralf Dahm. Briefly, zebrafish were raised on 14 h light 10 h dark cycle at 26.0  $\pm$  0.5°C. The embryos were obtained via natural mating and cultured in the water. The embryos were collected and placed into 24-well plates, every ten embryos per well. When the embryos older than 6 hpf, more than 50% epiboly, they were treated with 1, 5, 10  $\mu$ M of RA derivatives in E2 solution. The phenotypes were observed and images were captured using the Axio Scope A1 microscope system from Carl Zeiss at 24 and 72 hpf. All experiments in this study were carried out according to the ethical and welfare principles in legislation on animal research in Germany.

#### 4.3.6. *In vivo* scanning of the mouse retina

Mixed genders of homozygous mice expressing human mutant P301S tau, those were backcrossed for at least 7 generations to obtain animals on a pure C57Bl/6 background were used in this study. The ophthalmological examinations of the mouse retinas were performed using a modified Spectralis HRA + OCT system (Heidelberg Engineering, Dossenheim, Germany) like described elsewhere.<sup>17</sup> In short, mice received 24 h before the imaging sessions i.p. injections of the fluorescent probes (28-31 mM in DMSO). Imaging was performed using two different lasers wavelengths for the excitation of the fluorophores (450 and 488 nm). Emission filters used in this study were LP 458 nm, BP 512/25, BP 550/49 nm and BP 617/73 nm. To exclude false positive signals from retinal autofluorescence, pre-examinations of the retinas before the application of the fluorophores were performed.

### 5. Acknowledgement

This work was supported by grants from the German Federal Ministry of Education and Research (Bundesministerium für Bildung und Forschung, Germany, 13N10636) and the Hans and Ilse Breuer-foundation.

### 6. References and Notes

- Jakob-Roetne, R.; Jacobsen, H. *Angew. Chem. Int. Ed.* **2009**, *48*, 3030.
- Alzheimer's Association, *J. Alz. Assoc.*, 2012; Vol. March 2012, 131.
- Selkoe, D. *Physiol. Rev.* **2001**, *81*, 741.
- Clark, C.; Pontecorvo, M.; Beach, T.; Bedell, B.; Coleman, R.; Doraiswamy, P.; Fleisher, A.; Reiman, E.; Sabbagh, M.; Sadowsky, C.;

- Schneider, J.; Arora, A.; Carpenter, A.; Flitter, M.; Joshi, A.; Krautkramer, M.; Lu, M.; Mintun, M.; Skovronsky, D.; Group, A.-A. S. *Lancet neurol.* **2012**, *11*, 669.
- Klunk, W. E. *Neurobiol. Aging* **2011**, *32*, Supplement 1, S20.
- Clark Cm, S. J. A. B. B. J.; et al. *J. Am. Med. Assoc.* **2011**, *305*, 275.
- Camus, V.; Payoux, P.; Barré, L.; Desgranges, B.; Voisin, T.; Tauber, C.; La Joie, R.; Tafani, M.; Hommet, C.; Chételat, G.; Mondon, K.; de La Sayette, V.; Cottier, J.; Beaufils, E.; Ribeiro, M.; Gissot, V.; Vierron, E.; Vercouillie, J.; Vellas, B.; Eustache, F.; Guilloteau, D. *Eur. J. Nucl. Med. Mol. Imaging* **2012**, *39*, 621.
- Okamura, N.; Suemoto, T.; Furumoto, S.; Suzuki, M.; Shimadzu, H.; Akatsu, H.; Yamamoto, T.; Fujiwara, H.; Nemoto, M.; Maruyama, M.; Arai, H.; Yanai, K.; Sawada, T.; Kudo, Y. *J. Neurosci.* **2005**, *25*, 10857.
- Fodero-Tavoletti, M. T.; Okamura, N.; Furumoto, S.; Mulligan, R. S.; Connor, A. R.; McLean, C. A.; Cao, D.; Rigopoulos, A.; Cartwright, G. A.; O'Keefe, G.; Gong, S.; Adlard, P. A.; Barnham, K. J.; Rowe, C. C.; Masters, C. L.; Kudo, Y.; Cappai, R.; Yanai, K.; Villemagne, V. L. *Brain* **2011**, *134*, 1089.
- Matsumura, K.; Ono, M.; Kimura, H.; Ueda, M.; Nakamoto, Y.; Togashi, K.; Okamoto, Y.; Ihara, M.; Takahashi, R.; Saji, H. *ACS Med. Chem. Lett.* **2011**, *3*, 58.
- Takeuchi, J.; Shimada, H.; Ataka, S.; Kawabe, J.; Mori, H.; Mizuno, K.; Wada, Y.; Shiomi, S.; Watanabe, Y.; Miki, T. *Dement. Geriatr. Cogn. Disord.* **2012**, *34*, 112.
- Arriagada, P. V.; Growdon, J. H.; Hedley-Whyte, E. T.; Hyman, B. T. *Neurology* **1992**, *42*, 631.
- Rao, J.; Dragulescu-Andrasi, A.; Yao, H. *Curr. Opin. Biotechnol.* **2007**, *18*, 17.
- Koronyo, Y.; Salumbides, B. C.; Black, K. L.; Koronyo-Hamaoui, M. *Neurodegener. Dis.* **2012**, *10*, 285.
- Bolander, A.; Kieser, D.; Voss, C.; Bauer, S.; Schon, C.; Burgold, S.; Bittner, T.; Holzer, J.; Heyny-von Haussen, R.; Mall, G.; Goetschy, V.; Czech, C.; Knust, H.; Berger, R.; Herms, J.; Hilger, I.; Schmidt, B. *J. Med. Chem.* **2012**, *55*, 9170.
- Ono, M.; Watanabe, H.; Kimura, H.; Saji, H. *ACS Chem. Neurosci.* **2012**, *3*, 319.
- Schon, C.; Hoffmann, N. A.; Ochs, S. M.; Burgold, S.; Filser, S.; Steinbach, S.; Seeliger, M. W.; Arzberger, T.; Goedert, M.; Kretschmar, H. A.; Schmidt, B.; Herms, J. *PLoS one* **2012**, *7*, e35547.
- Bulic, B.; Pickhardt, M.; Schmidt, B.; Mandelkow, E.-M.; Waldmann, H.; Mandelkow, E. *Angew. Chem. Int. Ed.* **2009**, *48*, 1740.
- Bulic, B.; Pickhardt, M.; Khlistunova, I.; Biernat, J.; Mandelkow, E.-M.; Mandelkow, E.; Waldmann, H. *Angew. Chem. Int. Ed.* **2007**, *46*, 9215.
- Messing, L.; Decker, J. M.; Joseph, M.; Mandelkow, E.; Mandelkow, E.-M. *Neurobiol. Aging* **2013**, *34*, 1343.
- Ono, M.; Hayashi, S.; Matsumura, K.; Kimura, H.; Okamoto, Y.; Ihara, M.; Takahashi, R.; Mori, H.; Saji, H. *ACS Chem. Neurosci.* **2011**, *2*, 269.
- La Pietra, V.; Marinelli, L.; Cosconati, S.; Di Leva, F. S.; Nuti, E.; Santamaria, S.; Pugliesi, I.; Morelli, M.; Casalini, F.; Rossello, A.; La Motta, C.; Taliani, S.; Visse, R.; Nagase, H.; da Settimo, F.; Novellino, E. *Eur. J. Med. Chem.*, **2012**, *47*, 143.
- Augelli-Szafran, C., Elizabeth; Glase, S., Ann; Walker, L., Craswell; Yasunaga, T. Patent WO2000/76987, 2000.
- Chen, Y.; Li, C.; Zeng, Z.; Wang, W.; Wang, X.; Zhang, B. *Chem. Lett.*, **2005**, *34*, 762.
- Johnson, S. L.; Jung, D.; Forino, M.; Chen, Y.; Satterthwait, A.; Rozanov, D. V.; Strongin, A. Y.; Pellecchia, M. *J Med. Chem.*, **2006**, *49*, 27.
- Ohishi, Y.; Mukai, T.; Nagahara, M.; Yajima, M.; Kajikawa, N.; Miyahara, K.; Takano, T. *Chem. Pharm. Bull.* **1990**, *38*, 1911.

27. Narlawar, R.; Pickhardt, M.; Leuchtenberger, S.; Baumann, K.; Krause, S.; Dyrks, T.; Weggen, S.; Mandelkow, E.; Schmidt, B. *ChemMedChem*, **2008**, *3*, 165.
28. Gu, J.; Anumala, U. R.; Lo Monte, F.; Kramer, T.; Heyny von Haussen, R.; Holzer, J.; Goetschy-Meyer, V.; Mall, G.; Hilger, I.; Czech, C.; Schmidt, B. *Bioorg. Med. Chem. Lett.*, **2012**, *22*, 7667.
29. Gu, J.; Anumala, U. R.; Heyny-von Haussen, R.; Holzer, J.; Goetschy-Meyer, V.; Mall, G.; Hilger, I.; Czech, C.; Schmidt, B. *ChemMedChem*, **2013**, *8*, 891-897.
30. Uchihara, T.; Nakamura, A.; Yamazaki, M.; Mori, O. *Acta Neuropathol.* **2000**, *100*, 385.
31. Xia, C. F.; Arteaga, J.; Chen, G.; Gangadharmath, U.; Gomez, L. F.; Kasi, D.; Lam, C.; Liang, Q.; Liu, C.; Mocharla, V. P.; Mu, F.; Sinha, A.; Su, H.; Szardenings, A. K.; Walsh, J. C.; Wang, E.; Yu, C.; Zhang, W.; Zhao, T.; Kolb, H. C. *Alzheimers Dement.* **2013**.
32. Wager, T.; Chandrasekaran, R.; Hou, X.; Troutman, M.; Verhoest, P.; Villalobos, A.; Will, Y. *ACS Chem. Neurosci.* **2010**, *1*, 420.
33. Gasparini, L.; Crowther, R.; Martin, K.; Berg, N.; Coleman, M.; Goedert, M.; Spillantini, M. *Neurobiol. Aging* **2011**, *32*, 419.

**Graphical Abstract**

To create your abstract, type over the instructions in the template box below.  
Fonts or abstract dimensions should not be changed or altered.

**Fluorescent rhodanine-3-acetic acids  
visualize neurofibrillary tangles in  
Alzheimer's disease brains**

Leave this area blank for abstract info.

Upendra Rao Anumala<sup>a</sup>, Jiamin Gu<sup>a</sup>, Fabio Lo Monte<sup>a</sup>, Thomas Kramer<sup>a</sup>, Roland Heyny-Von Haußen<sup>b</sup>, Jana Hölzer<sup>c</sup>, Valerie Goetschy-Meyer<sup>d</sup>, Christian Schön<sup>e</sup>, Gerhard Mall<sup>b</sup>, Ingrid Hilger<sup>c</sup>, Christian Czech<sup>d</sup>, Jochen Herms<sup>e</sup>, Boris Schmidt<sup>a,\*</sup>

